PiR3D®, an effective and user-friendly 3D rockfall simulation software: formulation and case-study application

Y. Cottaz[1] — J.D. Barnichon[2] — N. Badertscher[3] — F. Gainon[3]

[1] *Geociel SA, 161 avenue Franklin Roosevelt, F-69150 Décines*
ycottaz@geociel.fr

[2] *Conseiller technique*
jdbarnichon@gmail.com

[3] *Institut Geotechnique SA, Les Places 38, CH-2855 Glovelier*
Info.ju@geo-online.com

ABSTRACT. Since the beginning of the 90's, various advances improved the comprehension of rock blocks – soil interactions, the development of algorithms describing their movement and the reconstruction of three-dimensional terrain models. However, few of them have concretised in easy-to-use tools by soils engineers dealing with rock hazards on a daily basis. Based on efficient three dimensional modelling algorithms, the PiR3D software was developed to fill this lack. A preliminary case study, carried out in the Jura Canton (Switzerland), illustrates its help to qualify risk zones and to locate and pre-dimension protection works.

RÉSUMÉ. Depuis le début des années 90, des avancées variées ont permis d'améliorer la compréhension des interactions blocs rocheux – sol, le développement d'algorithmes décrivant leur mouvement et la reconstruction de modèles de terrain tridimensionnels. Peu ont cependant abouti à la finalisation d'outils facilement utilisables par les praticiens du sol confrontés quotidiennement à l'évaluation de l'aléa rocheux. Basé sur des algorithmes de modélisation tridimensionnels performants, le logiciel PiR3D a été développé pour pallier ce manque. Un cas d'étude préliminaire, réalisé dans le Canton du Jura (Suisse), illustre l'aide apportée pour qualifier les zones de risque et implanter et pré-dimensionner des ouvrages de protection.

KEY WORDS: 3D rockfall modelling, probabilistic, hazard, risk, dimensioning.

MOTS-CLÉS: Modélisation de chute de blocs 3D, probabiliste, aléa, risque, dimensionnement.

1. Introduction

Since the beginning of the nineties, various advances have improved the comprehension of rock blocks – soil interactions, the development of algorithms describing their movement and more recently the reconstruction of three-dimensional terrain models. This gave rise to quite a number of computer codes (a review of these codes is given in Guzzetti *et al.*, 2002) to model rockfalls.

As far as two-dimensional (2D) analyses are concerned, worth mentioning the RocFall® commercial software (Stevens, 1998), widely used by engineering consultants. Although the use of such 2D codes is justified for studies in which the problem is essentially 2D, their use in cases deviating noticeably from this condition leads almost inevitably to inaccuracy in the predicted trajectories, so it becomes difficult to delimitate risk zones and to design protection works. Moreover, even the probabilistic approach than may be carried out with such 2D codes can be biased, as out of plane effects such as lateral dispersion and related unexpected events cannot be taken into account (Agliardi and Crosta, 2003). As an illustration, the comparison between 2D and 3D modelling of the M. Salta rockfall case study (Tagliavini *et al.*, 2009) showed significant differences between the 2D and the 3D approaches, an important one being that the 3D approach provides more conservative results.

Several research codes already exist for three-dimensional (3D) rockfall analysis, of which the codes STONE (Guzzetti *et al.*, 2002; Agliardi and Crosta, 2003) and RockyFor (Dorren *et al.*, 2006). However, few of them are really easy-to-use tools in daily applications for engineering consultants. Consequently, they are not commonly used for 3D rockfall studies to answer contractors (territorial collectivities or private owners) needs.

Although previously existing as a research code, the new version of the 3D rockfall simulation software PiR3D® was entirely redeveloped by Geociel SA to provide a software that could easily be used by engineering consultants (Cottaz and Faure, 2008). Its originality lies in its DTM representation, some specific numerical aspects and its versatility. The main aspects of the formulation used in PiR3D version 3.0 are detailed in the next section.

In the last section, a real preliminary case study, carried out in 2009-2010 in the Jura Canton (Switzerland) by Institut Geotechnique SA, illustrates how the software was used to qualify risk zones and to locate and pre-dimension protection works.

2. Overview of the PiR3D architecture and formulation

PiR3D has been designed as an intuitive fully integrated software, i.e. it handles most (if not all) steps involved in the desk part of rockfall studies. A deterministic modelling approach involves: i) the creation or import of meshes to model the 3D topography and to obtain a Digital Terrain Model (DTM), ii) the setting/attribution of soils to the DTM, iii) the definition of blocks source zones, iv) the definition of physical parameters to each soil, v) the trajectory computation, and last vi) the analysis tools required to extract information from the simulation rough results. In case a probabilistic approach is considered to compute block trajectories, uncertainty is further added at relevant locations in the process. The main ingredients of these aforementioned steps are detailed in the following parts of this section.

2.1. *Three dimensional model of topography*

PiR3D intrinsically works on meshes based on Triangular Irregular Network (TIN), but it can indeed handle Triangular Regular Network (TRN) meshes as well. This choice proves to give the best adaptability and accuracy to most surface mesh types. Additionally, it provides more flexibility than DEM based models in which blocks sources are restricted to cell centre (Agliardi *et al.*, 2003). However, the spatial location of geometrical objects (points, segments, faces) is much more CPU costly in TIN than in TRN-based meshes, especially if a naïve location is performed. This drawback is mitigated here by the use of a spatial locator based on a search tree (here a quadtree in the horizontal plane), for which the recursion depth is automatically adjusted depending on the mesh size.

As a result of the TIN mesh choice, the DTM can be created either from a mouse digitizing of level curves and topographic points provided a level-curves map is available, or from a direct file reading of topographic data (level curves, points) files under a wide range of formats such as xyz ascii (TXT), digital elevation model (DEM) and drawing exchange format (DXF). In all cases, the DTM surface is triangulated automatically from this dataset (either using a trivial or a Delaunay algorithm), which leads to the corresponding oriented TIN mesh. However, it is also possible to import directly oriented TIN meshes from existing DTM files for various file formats such as Stanford polygon (PLY), Stereolithography (STL) and AutoDesk 3ds Max (3DS). Additionally, a texture layer (aerial photo, map image…) can be mapped onto the DTM, which besides giving it more realism, also appears to be handy for the user in the next steps.

2.2. *Setting/attribution of soils to the DTM and definition of block sources*

At the end of the topography creation, the DTM contains a single default soil. Then, soils required to represent the site geology are imported from the soils library and their parameters can be adapted to the site specificities. Finally, each soil is assigned to the relevant DTM portion using an interactive mouse selection of either individual DTM faces or a group of faces. This operation is even made simpler if in the previous phase a map layer has been imported, from which the geology can be located and transposed to the DTM thanks to a transparency visual effect.

The position of block sources (no limit on their number) is set interactively as 2D polylines mapped onto the DTM. Each source is then attributed a number of blocks, an initial velocity or a fall height above topographic surface (in this case with a nil velocity), and a mass for individual blocks. Note that, as detailed in the following section, the block mass (*m*) does not enter in the trajectory computation. In fact, it is only used here to obtain a proper energy dimension of the output results.

2.3. *Physical formulation of the deterministic block trajectories computation*

Depending on the location of the block with respect the soil surface, the block position evolves with time along its trajectory following one of these two kinematics types: either free-fall in the air or rolling (sliding) on the soil surface. The impact of the block on the soil can be viewed as third type mostly characterized by energy dissipation, considered here as an almost instantaneous phenomenon (though this is not strictly true, see e.g. Pichler *et al.*, 2005) which, neglecting the indentation depth, occurs at a fixed position. For instance starting from a free-fall kinematics, the impact can either lead to bounce i.e. to a new free-fall trajectory portion, or to a change in kinematics type i.e. to a new rolling trajectory portion.

Thus, the trajectory is considered as a succession of kinematical phases (either flying or rolling) separated by purely dissipative phases (impacts). For each of these three phases, a lumped mass approach is used, i.e. the block reduces at point (nil size, shapeless) where the block mass *m* is concentrated.

2.3.1. *Formulation of the kinematical phases (free-fall and rolling)*

Similarly to other computer codes of this type, the trajectory kinematics modelling is based on the classical dynamic equilibrium relation

$$\sum \mathbf{F} = m \cdot \frac{d^2\mathbf{X}}{dt^2} \qquad [1]$$

where **F** is the forces vector, **X** the global spatial coordinates vector and *t* the time.

2.3.1.1. Free-fall kinematics

According to the lumped mass approach, the friction of the block in the air is neglected. Under these assumptions, the only force entering equation [1] is the block weight **P**, i.e. **F** = **P**. Using the gravity vector $\mathbf{g} = \{0,0,g\}$, with $g = -9.81\ m{\cdot}s^{-2}$, the weight thus writes $\mathbf{P} = m{\cdot}\mathbf{g}$ and equation [1] then simplifies to

$$\frac{d^2\mathbf{X}}{dt^2} = \mathbf{g} \qquad [2]$$

Let us consider a vertical plane that contains the initial velocity vector **V**, defined by a local reference frame $(0,x_1,x_3)$ with the $(0,x_3)$ axis defined upward. Projecting [2] on both axes, and integrating twice with respect to t taking into account the initial conditions at t=0 in velocity ($v_{(t=0)}$) and position ($x_{(t=0)}$) yields the well known projectile time equations (independent of the block mass), which defines a parabola

$$\begin{aligned} x_1(t) &= v_{1(t=0)} \cdot t + x_{1(t=0)} \\ x_3(t) &= \frac{1}{2} g \cdot t^2 + v_{3(t=0)} \cdot t + x_{3(t=0)} \end{aligned} \qquad [3]$$

To avoid a discrete time stepping scheme (based on [3]) for determining the impact position, the trajectory parametric equation (obtained from [3] by elimination of t) is combined with the parametric equation of the intersection polyline between the vertical plane $(0,x_1,x_3)$ and the DTM. This leads advantageously to a fully explicit solution for the impact position, from which the impact time t is obtained.

2.3.1.2. Rolling (sliding) kinematics

As a consequence of the used lumped mass approach, the rolling is not strictly currently considered (rotational velocities are undefined for a point), which is a conservative approach (Agliardi and Crosta, 2003). Thus, rolling is here equivalent to sliding. The block rolling onto the DTM surface is then represented by a dynamic Coulomb solid friction model that defines the frictional force **T** by

$$\begin{aligned} &\|\mathbf{T}\| = k \cdot \|\mathbf{N}\| && \text{a)} \\ &\mathbf{T}/\|\mathbf{T}\| = -\mathbf{V}/\|\mathbf{V}\| && \text{b)} \end{aligned} \qquad [4]$$

where k represents the dynamic friction coefficient, **N** the normal force acting on the surface and **V** the velocity in the plane (the out of plane velocity component being nil). Note that the frictional force vector **T** is collinear and opposite to **V** (Equation [4b]). Under these assumptions, the forces entering equation [1] are the block weight **P** and the rolling (sliding) friction **T**. Considering here a plane with slope angle α and the local reference frame (n,h,d) as shown in Figure 1, and noting that $V_\mathrm{n} = 0$, equation [1] then yields

$$\begin{aligned} \frac{d^2 X_\mathrm{h}}{dt^2} &= k \cdot g \cdot \cos\alpha \frac{V_\mathrm{h}}{\|\mathbf{V}\|} \\ \frac{d^2 X_\mathrm{d}}{dt^2} &= k \cdot g \cdot \cos\alpha \frac{V_\mathrm{d}}{\|\mathbf{V}\|} + g \cdot \sin\alpha \end{aligned} \quad \text{, with } \|\mathbf{V}\| = \sqrt{V_\mathrm{h}^2 + V_\mathrm{d}^2} \qquad [5]$$

Due to the term $\|\mathbf{V}\|$, these second order differential equations are coupled and cannot be integrated analytically. Here, they are integrated numerically over time using an adaptive 4th order Runge-Kutta-Nyström algorithm (a faster but less accurate Euler method was used in previous versions), using a modification of the method proposed by Lund *et al.* (2009). The adaptive time stepping scheme allows controlling the local integration accuracy (default value set at 10^{-3} m) on the trajectory position, and is stable even for trajectories deviating a lot from the dip direction. Whenever a specific spatial solution is required (e.g. apex or stopping point, or intersection point with a triangle face), this method is associated with a dichotomy algorithm.

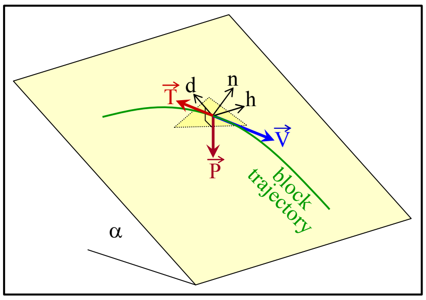

Figure 1. *Local reference frame used for the rolling formulation* (h: *face horizontal axis;* d: *face upward dip axis;* n: *face normal*).

2.3.2. *Formulation of the impact (purely dissipative phase)*

The impact of a flying block onto the soil surface is considered here as an instantaneous phenomenon for which the kinematics is almost nil. Thus it is mostly characterized by energy dissipation, which is accounted for in a classical way via restitution coefficients R_T and R_N, which are used to scale the local velocities (normal and tangential components with respect the surface at impact point).

2.3.3. *Transitions between types of kinematical phases (free-fall and rolling)*

Transitions between types of kinematical phases are defined by comparing the angle between the velocity and the DTM to a threshold angle β_{lim} (see Figure 2). In case of an incident (input) trajectory portion of:

– Free-fall (FF) type, the next portion (output) is a free-fall one if $\beta_{FF} > \beta_{lim}$ (case **a** in Figure 2) and a rolling one otherwise (case **b** in Figure 2), β_{FF} being the angle between $\mathbf{V}_{refl}$ and its vertical projection on the face. Energy dissipation is computed at impact in both cases;

– Rolling type (R), the next portion (output) is a rolling one if $\beta_R < \beta_{lim}$ or $\beta_{R'} < \beta_{lim}$ (cases **d** and **f** in Figure 2) and a free-fall one otherwise (see cases **c** and **e** in Figure 3), β_R and $\beta_{R'}$ being the angles between **V** and the vertical projection of **V** onto the neighbour face that **V** points to. Energy dissipation occurs only in case **e**.

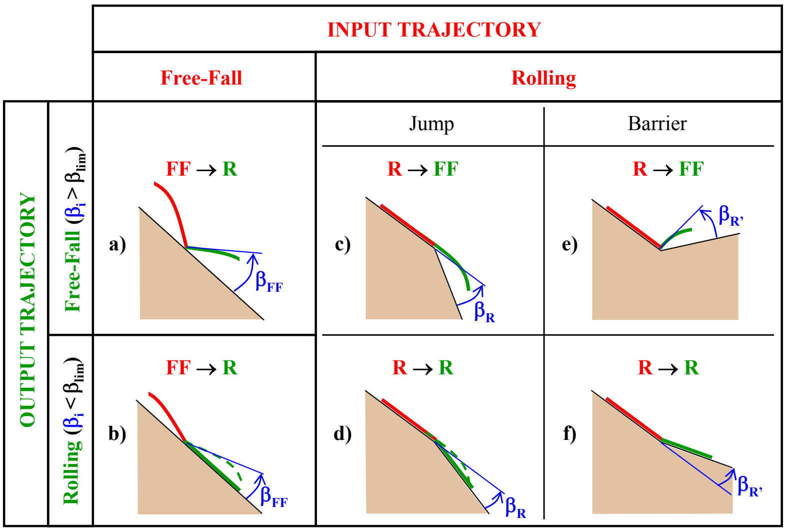

Figure 2. *Schematic of the different transition cases between Free-Fall* (FF) *and Rolling* (R) *trajectory portions,* β_i *corresponding either to* β_{FF}*,* β_R *or* $\beta_{R'}$.

2.4. *Integrating a probabilistic approach in block trajectories computation*

In the used probabilistic approach, up to five parameters can be set individually as being represented by probabilistic variables:

– Dynamic friction coefficient (k), normal (R_N) and tangential (R_T) restitution coefficients to account for the uncertainty about these parameters;

– Horizontal (θ_H) and vertical (θ_V) perturbations of rebound angles to take into account the uncertainty in the DTM representation of local slopes. These two perturbation angles define a rebound uncertainty cone with an ellipsoid base, centred on the reflected velocity direction given by R_N and R_T corrections.

Denoting ε the deterministic value of any of these five parameters, let us express its probabilistic value ε_P as

$$\varepsilon_P = \varepsilon + \mathcal{D}(d_\varepsilon) \qquad [6]$$

where $\mathcal{D}()$ is a given probability distribution of the parameter uncertainty d_ε, with d_ε depending on the incident velocity according to the following model

$$\begin{cases} if \left\|\mathbf{V}\right\| \le V_{\varepsilon(\mathrm{res})} \rightarrow d_\varepsilon = d_{\varepsilon(0)} + \dfrac{\left\|\mathbf{V}\right\|}{V_{\varepsilon(\mathrm{res})}}\left(d_{\varepsilon(\mathrm{res})} - d_{\varepsilon(0)}\right) \\ if \left\|\mathbf{V}\right\| > V_{\varepsilon(\mathrm{res})} \rightarrow d_\varepsilon = d_{\varepsilon(\mathrm{res})} \end{cases} \qquad [7]$$

This model makes it possible to account for a higher parameter uncertainty at lower velocity than at higher ones (see Figure 3). Indeed, it can be degenerated to a constant (i.e. velocity independent) model provided the condition $d_{\varepsilon(\mathrm{res})} = d_{\varepsilon(0)}$ is set.

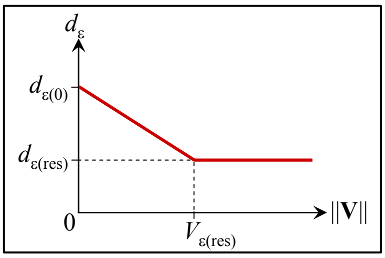

Figure 3. *Model of probabilistic parameters dependence on velocity.*

Two types of probabilistic simulations are accessible, for which the following particular forms of equation [6] are used:

– In the case of stochastic (or Monte-Carlo) simulations, the uniform probabilistic value $\varepsilon_{\mathrm{P(uniform)}}$ of any parameter ε is computed from

$$\varepsilon_{\mathrm{P(uniform)}} = \varepsilon + \Delta_\varepsilon \cdot \mathcal{U}(-1,+1) \qquad [8]$$

where Δ_ε is the parameter variation (equivalent here to d_ε), and $\mathcal{U}(-1,+1)$ the uniform distribution between -1 and $+1$ sampled from the *rand*() C++ function;

– If simulations based on a normal distribution are chosen, the Gaussian probabilistic value $\varepsilon_{\mathrm{P(Gaussian)}}$ of any parameter ε is obtained from

$$\varepsilon_{\mathrm{P(Gaussian)}} = \mu_\varepsilon + \sigma_\varepsilon \cdot \mathcal{N}(0,1) \qquad [9]$$

where μ_ε is the parameter mean (corresponding to ε), σ_ε its standard deviation (equivalent here to d_ε), and $\mathcal{N}(0,1)$ the standard normal distribution sampled from the Box-Muller transform (using *rand*() function calls).

Finally, the following sequence is applied in the probabilistic approach:

– For each rolling trajectory portion, a probabilistic value of k is computed and is used in Equation [5] to obtain the next trajectory point;

– For each dissipative impact (i.e. either with an incident or reflected FF portion, see Figure 2), probabilistic R_N and R_T values are used to compute reflected velocities. Then, probabilistic perturbation angles θ_H and θ_V are used to disturb the reflected velocities. These probabilistic corrections may lead to some trajectories penetrating inside the DTM, which is not geometrically acceptable. In such cases, the final reflected velocity is rotated to be set tangent to the soil face.

2.5. *Summary of the PiR3D parameters used to compute block trajectories*

Parameters required for each soil to compute block trajectories are summarized in Table 1. The last column parameters ($d_{\varepsilon(\mathrm{res})}$ and $V_{\varepsilon(\mathrm{res})}$) are only required if a velocity dependency of the parameters is chosen (equation [7]).

	Parameter	**Deterministic (ε)**	**Probabilistic**		
			Uniform (ε, Δ_ε)	**Gaussian (μ_ε, σ_ε)**	$d_{\varepsilon(\mathrm{res})}$, $V_{\varepsilon(\mathrm{res})}$
Free-fall	None	–	–	–	–
Rolling	Dynamic friction	k	k, Δk	μ_k, σ_k	$d_{k(\mathrm{res})}$, $V_{k(\mathrm{res})}$
Impact	Normal restitution	R_N	R_N, ΔR_N	$\mu_{R\mathrm{N}}$, $\sigma_{R\mathrm{N}}$	$d_{R\mathrm{N}(\mathrm{res})}$, $V_{R\mathrm{N}(\mathrm{res})}$
	Tangential restitution	R_T	R_T, ΔR_T	$\mu_{R\mathrm{T}}$, $\sigma_{R\mathrm{T}}$	$d_{R\mathrm{T}(\mathrm{res})}$, $V_{R\mathrm{T}(\mathrm{res})}$
	Horiz. perturbation	–	0, $\Delta\theta_\mathrm{H}$	0, $\sigma_{\theta\mathrm{H}}$	$d_{\theta\mathrm{H}(\mathrm{res})}$, $V_{\theta\mathrm{H}(\mathrm{res})}$
	Vert. perturbation	–	0, $\Delta\theta_\mathrm{V}$	0, $\sigma_{\theta\mathrm{V}}$	$d_{\theta\mathrm{V}(\mathrm{res})}$, $V_{\theta\mathrm{V}(\mathrm{res})}$
Transition	Threshold angle	β_{lim}	No	No	No

Table 1. *Parameters used in PiR3D to compute block trajectories.*

2.6. *Post-processing analysis tools*

Three types of post-processing analysis tools are integrated in PiR3D.

The first one is a display, for any trajectory, of its energy either as a profile along this trajectory or as a colour-scale mapped onto the trajectory (see Figure 12).

The next one is related to the possibility of emplacing protections (nets) on the MNT (see Figure 11). Then, taking into account all the blocks that effectively reached them, the following results are automatically displayed for each net: i) a developed view with block position and either energy (see Figure 11c) or height of the block impacts onto the net, and ii) an histogram representation of either energy (see Figure 11d) or height distribution on the net. Each net can be moved interactively and all the results are automatically updated.

The last type makes it possible to build different envelope maps from all trajectories using a user-defined grid, currently: velocity, energy (see Figure 9), energy classes, height above MNT, stopping points and density (i.e. number of trajectories crossing each cell divided by the overall number of trajectories).

3. Application to a real case study in the Jura Canton (Switzerland)

The Jura Canton is localised in the Jura Mountains, a small mountain range located north of the north-western Alps, at the front of the Molasse plateau. The Jura fold and thrust belt forms an arcuate structure where Mesozoic and Cenozoic layers are folded and thrusted over an evaporitic decollement layer at the base of the

Triasic rocks. The studied area is located between the cities of Delémont and Moutier (see Figure 4). The main road between these two cities crosses the Moutier Gorges that cuts several anticlines, of which subvertical limbs form limestone cliffs. Folding and thrusting of these rocks has resulted in their fracturation. Rockfall hazard exists along this road and therefore protection works are planned. In order to determine the types of protection works, a study of the risk associated with rockfall hazard has been asked by the authorities of the Jura Canton. To determine this risk, intensity maps of rockfall hazard along the road have to be elaborated. Falling blocks have very variable sizes in the study area mainly depending on geological features (fracturation, lithology). Preliminary results of the trajectory computations are presented here.

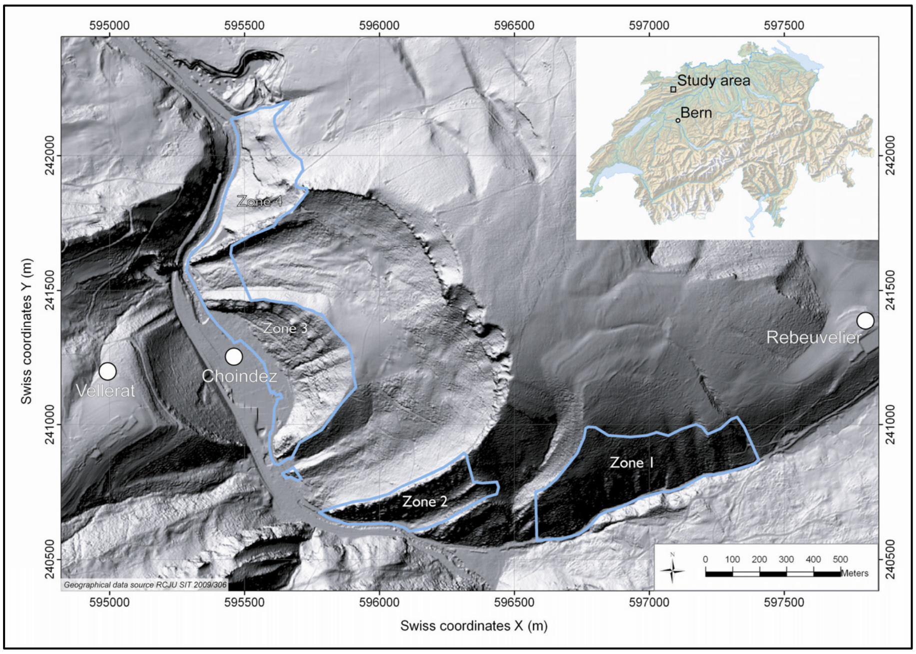

Figure 4. *Map of the studied area (geographical data source RCJU SIT 2009/306).*

3.1. ***Definition of the study***

3.1.1. *Creation of the DTM*

The DTM has been provided by the authorities of the Jura Canton as a xyz file coming from the geographical data source RCJU SIT 2009/306. A two meters grid DTM has been used in this preliminary study. It has been imported and a topographic map superimposed on it to ease visualisation.

3.1.2. *Definition of soils and their associated parameters*

According to the field observations and geology, six soil types were created depending on vegetation density, rock alteration, rock types (marls/limestones) and presence of scree: sane rock, altered rock, soft soil, very soft soil, scree, high density vegetation soil. Soft soil corresponds to forest with humus. Very soft clayish soil is associated with altered Oxfordian marls and humid zones (swamps). Calibration of soil parameters (coefficients R_N and R_T, threshold angle β_{lim} and friction coefficient k) has been carried out in two steps. A first determination was based on available information provided by RocFall and PiR3D (existing default soils). To take into account the presence of forest, R_T has been reduced.

Then, rockfall simulations were performed and soils parameters iteratively adapted until trajectories fit as closely as possible existing field information such as:

– Extension of deposit zones: where possible (absence of dense vegetation), the presence of deposited blocks has been observed during field inspection. Thus, soil parameters have been adapted so that trajectories reach deposit and do not extend much further. For example, soils parameters have been adapted so that blocks cannot climb up on the other side of the valley;

– Known events: only few events are fully documented (block size, deposit zone, damages), but the Road Maintenance Service was able to provide information on frequency and zonation of rockfall on the road and associated block size. For example, they were able to indicate locations where only rare blocks reached the road, in opposition with zones where blocks reached the road very frequently. Soil parameters have thus been adapted to fit with these observations;

– During removing of very unstable blocks in cliffs, trajectories have been observed. Soil parameters have thus been adapted so that computed trajectories look like real ones. Especially, very high rebounds after impacting a subhorizontal surface have been corrected.

Table 2 gives the R_T and R_N parameters based on the initially available information and after trajectories fitting. The constant parameters considered in the iterative fit are summarized in Table 3.

	Input data in step 1		**Resulting data from step 2**	
Soil type	R_N	R_T	R_N	R_T
Sane rock	0.42	0.88	0.45	0.87
Altered rock	0.47	0.55	0.42	0.75
Soft soil	0.31	0.80	0.32	0.67
Very soft soil	0.30	0.79	0.30	0.52
Scree	0.31	0.81	0.33	0.71
Vegetated soil	0.31	0.82	0.30	0.60

Table 2. *Soil parameters estimation before (step 1) and after the iterative fit (step 2).*

<table>
<tr><th>Soil type</th><th>Δ_R [%]</th><th>$d_{R(\mathrm{res})}$ [%]</th><th>$V_{R(\mathrm{res})}$ [m/s]</th><th>Δ_θ [°]</th><th>$d_{\theta(\mathrm{res})}$ [°]</th><th>$V_{\theta(\mathrm{res})}$ [m/s]</th><th>k [-]</th><th>Δ_k [%]</th><th>$d_{k(\mathrm{res})}$ [%]</th><th>$V_{k(\mathrm{res})}$ [m/s]</th><th>$\beta_{\lim}$ [°]</th></tr>
<tr><td>Sane rock</td><td>4</td><td>2</td><td rowspan="6">10</td><td>0</td><td rowspan="6">10</td><td>5</td><td>0.50</td><td>12</td><td rowspan="6">10</td><td rowspan="6">10</td><td>2</td></tr>
<tr><td>Altered rock</td><td>5</td><td>3</td><td>10</td><td>10</td><td>0.55</td><td rowspan="5">15</td><td>4</td></tr>
<tr><td>Soft soil</td><td>10</td><td>6</td><td rowspan="4">20</td><td rowspan="4">15</td><td>0.65</td><td>7</td></tr>
<tr><td>Very soft soil</td><td>12</td><td>8</td><td>0.75</td><td>8</td></tr>
<tr><td>Scree</td><td>8</td><td>4</td><td>0.60</td><td>6</td></tr>
<tr><td>Vegetated soil</td><td>12</td><td>8</td><td>0.70</td><td>7</td></tr>
</table>

Table 3. *Soil parameters used in the stochastic simulations (also prescribed for the iterative fit detailed in §3.1.2), in addition to R_N and R_T parameters given in Table 2. Note that similar uncertainty on R_N and R_T (denoted here as R), and similar perturbation angles θ_H and θ_V (denoted here as θ) are considered here.*

3.1.3. *Attribution of soils to the DTM*

The specified soils have been attributed to the DTM model according to field observations. The soil repartition is only valid in the perimeter where rockfall occurs. Out of this perimeter, a default soil value has been set (see Figure 5a).

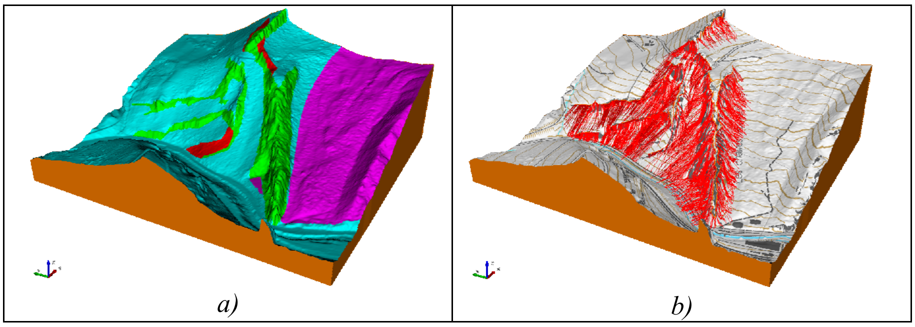

Figure 5. *a) Soils attributed to the DTM (green: sane rock; red: altered rock; light blue: soft soil; purple: very soft soil); b) Example of computed trajectories (light red: free-fall; dark red: rolling) (geographical data source RCJU SIT 2009/306).*

3.1.4. *Positioning of starting block lines*

During field inspection, two types of rockfall sources have been identified: single blocks and diffuse zones with homogeneous block size for a defined probability of mobilisation. Such heterogeneity of rockfall sources could easily be taken into account defining variable source sizes in the same calculation. Thus, single blocks have been positioned in the model as lines of minimal length with a single block starting, whereas diffuse zones have been implemented as lines with 50 to 100 falling blocks. Sources have been positioned at hand with the mouse in the 2D view by controlling their positions in the 3D view. To estimate the maximal possible energy of impacts, the lines were positioned at the top of cliffs/zones.

3.2. *Trajectory computations and analysis*

3.2.1. *Trajectory computation*

For zone sources, variable block sizes are attributed to probability of mobilisation, i.e. falling of large blocks is less frequent than falling of small stones. During field inspection, blocks size for return period 10, 30, 100 and 300 years have been estimated for each homogeneous zone. A trajectory computation has then been performed for each return period, attributing the determined block size for each source. To test the system variability, several computations (up to 30) were made with the true stochastic probabilistic option. Computations have then been compared to discard the non representative trajectories. Trajectories were considered as non representative when exhibiting an abnormal extension or path compared to other trajectories and when not reproduced through several computations. It does not mean that these trajectories are rejected but they are not considered for dimensioning the protection works, as it would result in an over-dimensioning of the latter. Such trajectories belong to the residual risk domain. The 3D simulation has evidenced channels that concentrate blocks where specific attention must be paid.

3.2.2. *Envelope analysis*

For each sector about 0.5 km^2 in area, a grid of 100×100 cells was chosen for the envelope calculation (resolution of 5-10 m), which is reasonable according to the block size and DTM resolution. The energy envelope is computed with PiR3D (Figure 6a) and the risk calculation with the Econome 1.0 software, in which intensity is provided in 3 classes: low (<30 kJ), medium (30-300 kJ) and high (>300 kJ) (www.econome.admin.ch). For each sector and return period, the energy envelope calculation was performed several times. Based on these maps (Figure 6b), the hazard intensity maps have then been elaborated for each return period.

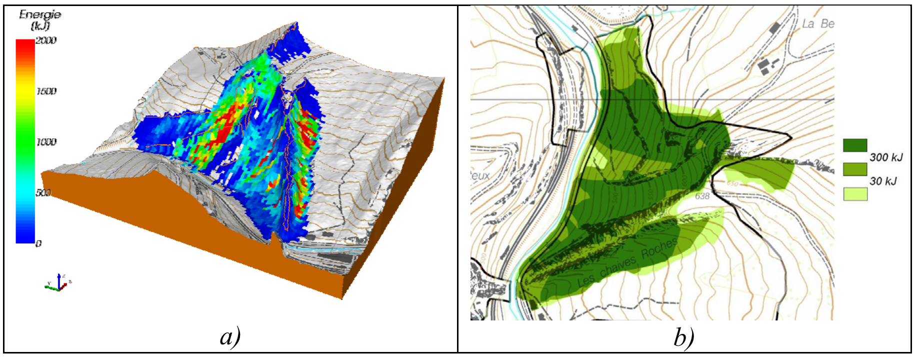

Figure 6. *Example of a computed energy envelope (left) and energy intensity map (right) (geographical data source RCJU SIT 2009/306).*

3.3. *Positioning and pre-dimensioning of protection works*

When rockfall occurs on regular topography, the positioning of rockfall barriers and catch fences can be performed with a 2D trajectory simulation. In the studied area, the topography is variable, sometimes on short distances. This results in variable and important rebounds, especially on cliff walls, and thus careful positioning of protection works is needed. Their first positioning was based on field observation, such as presence of channel, stepping stone… By analysing the energy of blocks and percentage of stop of these barriers, it was tried to optimize the number and type of rockfall barriers, and to see if stabilization measurements could be a better solution. The energy analysis of blocks on a net was performed with the analysis tool (see Figure 7). It showed that in some cases, the stabilisation of local zone above the net allows a drastic reduction of energy in the latter. E.g. Figure 7 shows that a single block has energy higher than 400 kJ (see Figure 8 for details). In such case, it is more justified to stabilize this block than to raise the fence energy on its whole length. The easy modelling procedure made it possible to obtain, in a relatively short time, a general protection concept that takes into account 3D topographic variability.

4. Conclusions

Fundamentals of PiR3D formulation have been presented. Using MNT either as TIN or TRN meshes, the deterministic approach is based on a lumped mass approach to formulate free-fall, rolling (sliding) and impact equations. Uncertainty can be accounted for using a probabilistic approach, which is applied on the main model parameters with a possible dependence on the block velocity. Moreover, several analysis tools are incorporated in the software.

PiR3D has been used by Institut Geotechnique for a 3D rockfall study in Switzerland, using its own experience previously gained with other 2D simulation softwares. Its easy use allowed determining risk and hazard zones in a short amount of time, and also to locate and pre-dimension protection works, which was one the challenging point.

Improvements are currently being developed, just to mention as a few:

– A massive simulation mode, which allows throwing an unlimited number of blocks (current limit is around 50 000 blocks), and thus investigating very low probability rockfall hazards;

– Addition of the uncertainties related to the source initial conditions (block mass, initial position and initial velocities), of rotational velocities in the formulation, of a dependence of R_T on the block size and on the slope roughness, and addition of a threshold normal velocity for free-fall to rolling transitions.

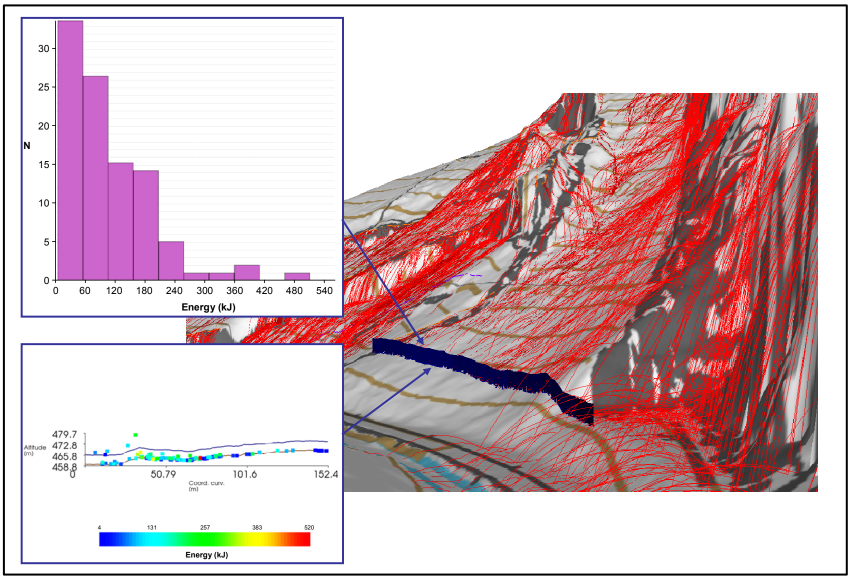

Figure 7. *Example of computed trajectories with position of a 6 m height net (shown in dark blue), location of impacts and related energy on the net (bottom left), energy distribution of the impacts arriving on the net (top left) (geographical data source RCJU SIT 2009/306).*

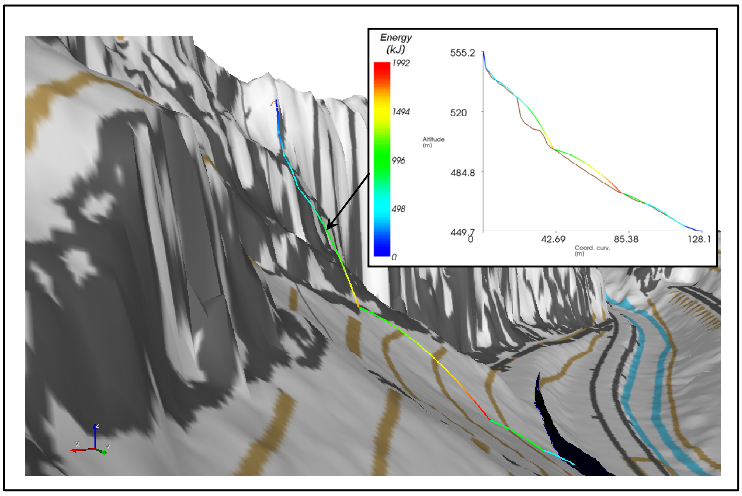

Figure 8. *Details of the highest energy (>400 kJ) trajectory: 3D view with energy mapped on the trajectory and energy mapped on the 2D trajectory profile (top right) (geographical data source RCJU SIT 2009/306).*

Acknowledgements

The authors would like to thank the authorities of the Republic and Canton of Jura who have allowed the publication of the preliminary results given in section 3.

5. References

Agliardi F., Crosta G., "High resolution three-dimensional numerical modelling of rockfalls", *International Journal of Rock Mechanics & Mining Sciences*, vol. 40, 2003, p. 455-471.

Cottaz Y., Faure R.M., "Pir3D, an easy to use three dimensional block fall simulator", *Proceedings of the 10th International Symposium on Landslides and Engineered Slopes*, Chen et al. (eds) ISBN 978-0-415-41196-7, 2008, p. 319-322.

Dorren L.K.A, Berger F., Putters U.S., "Real-size experiments and 3-D simulation of rockfall on forested and non-forested slopes", *Natural Hazards and Earth System Sciences*, vol. 6, 2006, p. 145-143.

Guzzetti F., Crosta G., Detti R., Agliardi F., "STONE: a computer program for the three-dimensional simulation of rock-falls", *Computer & Geosciences*, vol. 28, 2002, p. 1079-1093.

Lund E., Bugge L., Gavrilenko I., Strandlie A., "Track parameter propagation through the application of a new adaptive Runge-Kutta-Nyström method in the ATLAS experiment", *Journal of Instrumentation*, vol. 4, 2009, p. 1-15.

Pichler B., Hellmich Ch., Mang H.A., "Impact of rocks onto gravel. Design and evaluation of experiments", *International Journal of Impact Engineering*, vol. 31, 2005, p. 559-578.

Stevens W., "RocFall: a tool for probabilistic analysis, design of remedial measures and prediction of rockfalls", M.A.Sc. Thesis, 1998, University of Toronto.

Tagliavini F., Reichenbach P., Maragna D., Guzzetti F., Pasuto A., "Comparison of 2-D and 3-D computer models for the M. Salta rock fall, Vajont Valley, northern Italy", *Geoinformatica*, vol. 13, 2009, p. 323-337.